Journal of Materials Chemistry A

Accepted Manuscript

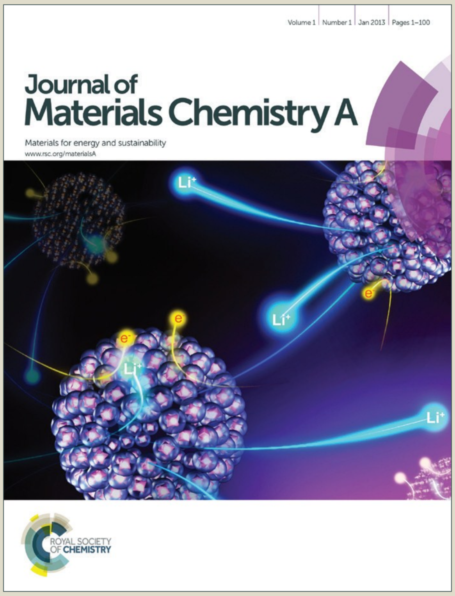

Volume 1 | Number 1 | Jan 2013 | Pages 1–100

Journal of Materials Chemistry A

Materials for energy and sustainability

www.rsc.org/materialsA

ROYAL SOCIETY OF CHEMISTRY

This is an *Accepted Manuscript*, which has been through the Royal Society of Chemistry peer review process and has been accepted for publication.

Accepted Manuscripts are published online shortly after acceptance, before technical editing, formatting and proof reading. Using this free service, authors can make their results available to the community, in citable form, before we publish the edited article. We will replace this *Accepted Manuscript* with the edited and formatted *Advance Article* as soon as it is available.

You can find more information about *Accepted Manuscripts* in the Information for Authors.

Please note that technical editing may introduce minor changes to the text and/or graphics, which may alter content. The journal's standard Terms & Conditions and the Ethical guidelines still apply. In no event shall the Royal Society of Chemistry be held responsible for any errors or omissions in this *Accepted Manuscript* or any consequences arising from the use of any information it contains.

ROYAL SOCIETY OF CHEMISTRY

www.rsc.org/materialsA

Journal of Materials Chemistry A

ARTICLE

Self-activated continuous pulverization film: an insight into the mechanism of extraordinary long-life cycleability of hexagonal $H_{4.5}Mo_{5.25}O_{18}·(H_2O)_{1.36}$ microrods†

Received 00th January 20xx,
Accepted 00th January 20xx

DOI: 10.1039/x0xx00000x

www.rsc.org/

Zihua Li,[ab] Hai Wang,[*ab] Zhuangzhi Sun,[ab] Jian Su,[ab] Zuyun Wang[c] and Linjiang Wang[ab]

For large amounts of transition metal oxides, sulfides and carbon group (IVA), the pulverization of electrodes materials in lithium-ion batteries (LIBs) is always a serious and common problem due to volume expansion and stress accumulation resulting from the phase transformation or alloying during the charge-discharge process, which leads to the capacity fading and thus limits LIBs's cycling performance. To solve these problems, conventionally, the rational design of electrode materials is needed. Here in this work, we report a novel anode material, hexagonal $H_{4.5}Mo_{5.25}O_{18}·(H_2O)_{1.36}$ microrods (HM) via a simple hydrothermal method. During the lithium-ion insertion/desertion process of HM, it was found that HM are drastically first transformed into Li_2MoO_4 nanotubes and then Li_2MoO_4 nanowire clusters embedded in amorphous sphere cages with Li_2O matrix, Mo metal and SEI thin film. Surprisingly, we discovered that HM exhibit extraordinary long-life cycleability with an unusual phenomina: specific capacity first decreased then increased. The outstanding electrochemical performance could be explained by the formation of intermediate phase Li_2MoO_4 nanowires and amorphous sphere cages, which can maintain lithium-ion paths and electronic transport, and prohibit the mechanical and chemical degradation of electrode materials. The results show that the pulverization of the HM anode materials induced by lithium-ion insertion-extraction played a trigger role in formation of continuous pulverization film. Accordingly, a "damage-reconstruction" model based on the *ex-situ* XRD and FESEM analysis combined with *ex-situ* XPS, FTIR and TEM characterizations upon the charge-discharge process was proposed to explain such an unusual and intriguing finding. Compared with the conventional method of preventing electrode materials from the pulverization, the robust continuous gel-like pulverization film containing unique combination of intermediate phase and amorphous sphere cage provides a new insight into the mechanism of extraordinary long-term cycleability of electrode materials.

Introduction

It is well-known that the pulverization of electrode materials in lithium-ion batteries (LIBs) is always a serious and common problem for the future commercial application of LIBs, especially for most transition metal oxides, sulphides and carbon group (IVA), e.g., MoO_3,[1-5] SnO_2,[6-8] $NiCo_2O_4$,[9-11] Sn,[12-15] Ge,[16-18] Si[19-21] and so on. Generally speaking, the reason of pulverization involved two main factors of the volume expansion and the phase transformation during the charge-discharge process. Especially for transition metal oxides electrode materials, the amorphous metal nanoclusters, Li_2O and SEI layer are unavoidable during the lithium-ion insertion/desertion process.[5, 7, 10, 17] Usually, these pulverized powders will drop off, detached, and are not connected to each other after long cycling (Scheme 1a). To prevent electrode materials from pulverizing, based on the analysis of a large amount of previous literatures and the basic principle of pulverization of electrode materials, it can be concluded that exploring novel electrode materials is needed. For example, the structural design includes one-dimensional and mesoporous structure of active materials, the hybrid composites, such as carbon materials and graphene and other novel structures, and so on.[1, 5, 7-9, 20, 22-24]

An accepted fact is that almost all the electrochemical reaction of electrode materials mentioned above were involved with great volume change. In this regard, therefore, how to connect different particles and to make them stable will be very crucial for maximizing the performance with long cycle life. In our study, Scheme 1b proposed a new concept of interconnecting pulverization particles. In this concept of proof, the pulverized powders were held together closely. Moreover, the pulverized powders can be self-activated with lithium-ion insertion/desertion, and finally formed continuous robust film. This pulverization film has at least three advantages for long-life LIBs application: (1) the film is robust without any detach occurring with long-life cycles; (2) lithium-ion insertion and desertion are confined within the continuous film without large

---

[a] College of Materials Science and Engineering, Guilin University of Technology, Guilin 541004, China, E-mail:hbwanghai@gmail.com; Fax: +86-773-5896-671;Tel: +86-773-5896-672.
[b] Key Laboratory of New Processing Technology for Nonferrous Metals and Materials, Ministry of Education, Guilin University of Technology, Guilin 541004, China.
[c] College of Civil Engineering and Architecture, Guilin University of Technology, Guilin 541004, China.

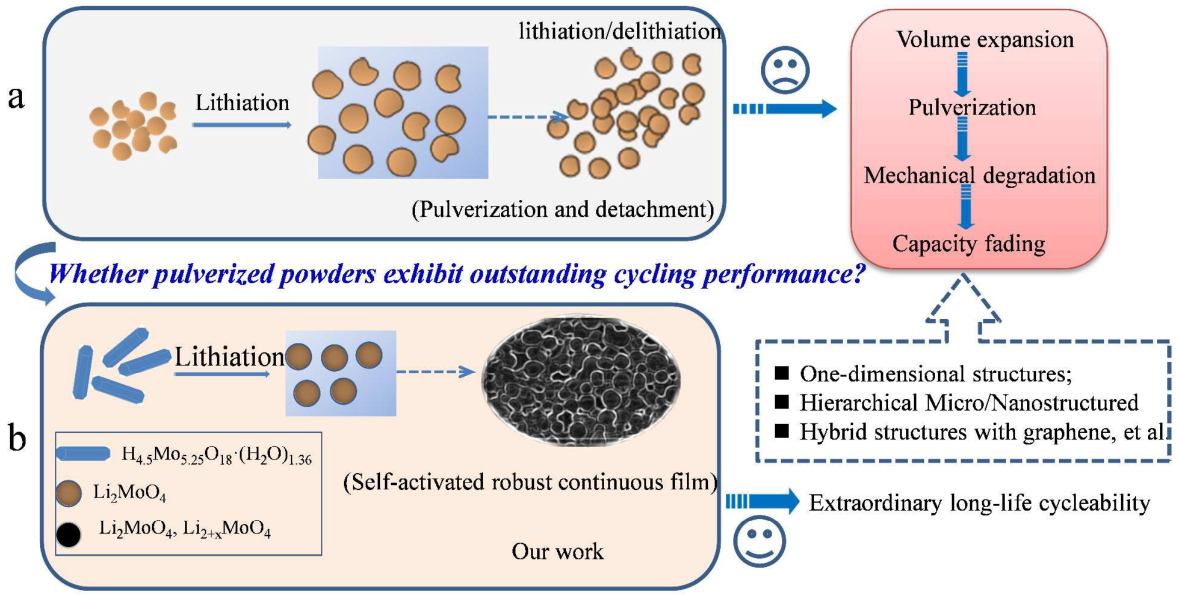

Scheme. 1 (a) The schematic illustration of the mechanism of electrode materials was pulverized and its corresponding solution; (b) the schematic illustration of the formation process of self-activated robust continuous film based on HM electrodes.

lithium-ion loss; (3) the enhanced large surface area of electrode materials driven by pulverization method will further provide more active sites for lithium-ion insertion/desertion.

MoO_3, as a promising electrode material, has been extensively investigated by many groups due to its unique layer structure and high theoretical capacity in LIBs application.[1-4] However, its relatively low specific capacity still lies behind of its practical application. Very recently, we demonstrated that H_xMoO_3, belonging to $M_xMoO_3\cdot nH_2O$, is more superior electrode material when compared with MoO_3, due to its metallic and layer structure features.[25] Over the past two decades, hexagonal molybdates with the general formula, $M_y\cdot zH_2O$, $Mo_{6-x}O_{18-x}H_{4x-y}$ had been reported.[26] From the perspective of crystal structure, actually, the most distinguishing structural feature of hexagonal molybdates is a wide one-dimensional tunnel (3.2-3.5 Å in diameter), which should allow lithium-ions free intercalation.[26] However, their LIBs performance and corresponding electrochemical mechanism are still uncertain. Actually, large amounts of space of above mentioned materials for lithium-ion insertion and desertion is ideal for the design of electrode materials. The unique and wide one-dimensional tunnel motivated us to explore synthesis and energy storage performance of new molybdenum-related materials. Some similar molybdates materials had already been reported, such as $(NH_4)Mo_{5.3}O_{17.3}H_{1.7}\cdot 0.4H_2O$, $Na_{1.0}Mo_{5.35}O_{17.35}H_{1.6}\cdot 1.7H_2O$ and so on, and their corresponding electrochemical properties were preliminarily investigated.[26] Although some similar materials, such as $(H_3O)_yMoO_3\cdot zH_2O$ was obtained by typical two steps, including the formation of sodium form and multiple acid treatment, to the best of our knowledge, $H_{4.5}Mo_{5.25}O_{18}\cdot(H_2O)_{1.36}$ is rarely reported to date.[26] Therefore, it is also highly desired for the facile synthesis of hexagonal $H_{4.5}Mo_{5.25}O_{18}\cdot(H_2O)_{1.36}$.

Here, we had synthesized $H_{4.5}Mo_{5.25}O_{18}\cdot(H_2O)_{1.36}$ microrods (HM) for the first time via a simple one-step hydrothermal method with assistance of PVP and formic acid. In our work, we take HM as a typical case, and address the concept of connecting pulverized particles for the first time. As a result, when tested as anode materials in LIBs, we found that this novel anode material was an ideal electrode material： high capacity (initial capacity 2072 mAh g^{-1}), fantastic long life span (without fade even up to 1000 cycles) and superior rate performance. To reveal the relationship between the microstructure and electrochemical performance, especially cycle performance, we use *ex-situ* XRD and FESEM combined other characterization, such as XPS, TEM and FTIR and so on, to investigate their electrochemical mechanism. Astonishingly, we discover that the extraordinary long-term cycleability of HM may be attributed to the formation of robust continuous pulverization gel-like film. The damage of HM and reconstruction of intermediate Li_2MoO_4 nanowires within the spheres of amorphous Mo metal, Li_2O matrix and SEI thin film may be critical factors for this unusual phenomenon.

Experimental section

Materials synthesis

All reagents were analytical grade and used without any further purification. In a typical synthesis, 30 mL of formic acid was slowly added to an aqueous solution of PVP (1 g of PVP dissolved in 30 mL of deionized water) in a flask under vigorous stirring. After being continuously stirred for 30 min in the flask, 1 g of ammonium molybdate $(NH_4)_6Mo_7O_{24}\cdot 4H_2O$ powder was added to the above mixture solution and continuously stirred another 30 minutes. Finally, the resultant suspension was transferred to a Teflon-lined stainless steel autoclave (100 mL volume) for hydrothermal treatment at 180 ℃ for 6 h. The autoclave was cooled to room temperature; the blue precipitates were collected by means of centrifugation, washed several times with deionized water and ethanol, and then dried in a vacuum at 70 ℃ for 24 h. To explore the role of formic acid, PVP and deionized water in forming the HM, in a control experimental, no water, no PVP and no formic acid was investigated, respectively. Specially, the HM with different volume ratio of formic acid and H_2O is denoted as HM-10, HM-20, HM-30. 10, 20, and 30 are different formic acid volume, respectively. Total volume of formic acid and H_2O remains 60 mL.

Material characterizations

The crystal structure was performed by X-ray diffraction (XRD) analysis with a PANanalytic X'Pert spectrometer using Cu Kα radiation, λ=0.15405 nm. The high-resolution transmission electron microscopy (HRTEM) images were obtained with a JEOL JEM-2010F microscopy operating at 200 kV. X-ray photoelectron spectroscopy (XPS) spectra were performed to analyse the surface of samples at different charge-discharge stages on an ESCALAB210 spectrometer using Al anode K_α (hν=1,486.61 eV) radiation as excitation source of monochromatical X-ray in ultrahigh vacuum (UHV) with a base pressure of 10^{-10} mbar. Fourier transform infrared (FTIR) absorption spectra were recorded on a Nicolet 6700 spectrometer (Thermo Fisher Scientific Inc., USA) from 4000 to 500 cm^{-1} using KBr pellets as dispersant. The specific surface area was measured by the Brunauer-Emmett-Teller (BET) approach using adsorption data over a relative pressure range, while pore size and its distribution was calculated by the Barrett-Joyner-Halenda (BJH) method based on the obtained desorption curves.

Electrochemical measurements

The electrochemical measurements were carried out using CR2025-type coin cells with pure lithium metal as both the counter electrode and the reference electrode at room temperature. The working electrode consisted of active material, a conductive agent (carbon black, Super-P-Li), and a polymer binder (poly(vinylidene difluoride), PVDF, Aldrich) in a 70 : 20 : 10 weight ratio. A Celgard 3400 membrane was used as a separator and 1.0 M $LiPF_6$ in a mixture of ethylene carbonate-diethyl carbonate (1 : 1 volume, Novolyte Technologies, USA) was used as the electrolyte. Cell assembly was carried out in an Ar-filled glovebox with concentrations of moisture and oxygen below 1.0 ppm. The charge/discharge cycling and cyclic voltammetry (CV) (0.01-3 V, 0.2 mV s^{-1}) was performed at room temperature using an electrochemical workstation (CHI 860 D, Beijing) using a battery testing system (NEWARE) at different current rates with a voltage window of 0.01-3 V. Electrochemical impedance spectroscopy (EIS) measurements were performed at frequencies ranging from 10^{-2} to 10^5 Hz.

Results and discussion

In a control experiment, it is obviously observed that the PVP, formic acid and H_2O play a critical role for synthesizing one-dimensional HM, as shown in Fig. 1a-d. Interestingly, we also found that the volume ratio of formic acid and H_2O had an obvious effect on the aspect ratio of HM, as shown in Scheme. S1. Considering that the importance of unique structural feature of one-dimensional architecture for LIBs application, e.g., $ZnFe_2O_4$ microrods,[27, 28] we take hexagonal microrods as our investigation samples. To clarify the concept of proof, HM-30 was taken as anode materials case in our work.

The corresponding XRD of HM-30 is shown in Fig. 1e. This result agrees with the PDF: 83-1176. An obviously crystal structure feature is its one-dimensional tunnel (Fig. 1e inset). MoO_6 is basic building unit. In our previous reports, H_xMoO_3 is a metal semiconductor with blue color due to the co-existence of mixture of Mo^{5+} and Mo^{6+} (Fig. 1e inset). PVP may play the role of a weak reduction agent during the reaction process, which has been reported in previous literature.[29-33] The mixture valence of transitional metals had been demonstrated to have a positive effect on the electrochemical performance, e.g., V, Ti.[34-38] The object of our work is to investigate their electrochemical properties of HM-30 with both one-dimensional microstructure and tunnel structure. Therefore, we expected that the lithium-ion should insert and desert into the tunnel freely like shuttle bus. Moreover, the crystal structure should be well retained. More lithium-ions would be easily intercalated into HM-30, and provide higher specific capacity. The expected good results are mainly based on the consideration of the following three factors: (1) the HM-30 structure wide one-dimensional pathway for lithium-ion diffusion; (2) the mixture valence of Mo^{5+} and Mo^{6+} will provide good conductivity; (3) the one-dimensional microstructure will provide fast electron transfer. First, we tested the cycling performance of HM-30 at 1 A g^{-1}. As shown in Fig. S1b, we found that the initial specific capacity is high up to 1637 mAh g^{-1}. Surprisingly, we found that the specific capacity of HM-30 sharply decreased to 152 mAh g^{-1} after 100 cycles, and then continuous increased. Furthermore, we evaluated the reproducibility of electrochemical performance of the HM-30 by another batch of sample, tested at different current density, 0.5, 1 and 2 A g^{-1} under the same conditions as described above (Fig. S1). The trend of specific capacity changes is similar: first quick fading, then continuous increasing. The unusual finding of HM-30 motivated us to explore the cycling performance of other HM-10 and HM-20, as shown in Fig. S2 and Fig. S3, respectively. The cycling performance results show that the phenomenon is similar to HM-30. The performance results of the three samples, HM-10, HM-20 and HM-30 are compared in Tab. S2. We noted that there is also a similar phenomenon in previous literature. A possible explanation is reactivation process of active materials themselves during the charge-discharge process.[39, 40] Very recently, a high-rate lithiation-induced reactivation of mesoporous hollow spheres for long-lived lithium-ion batteries was reported by Lian group. Lian et al found that the capacity first faded and then increased by finely tunning mesoporous structure of the metal oxide sphere and optimizing stable solid-electrolyte interface (SEI) by high-rate lithiation-induced reactivation.[41] In our HM-30 case, such a quite unusual and intriguing finding, we decided to further focus on its microstructure and phase transformation as a function of different stages of cycles so as to obtain valuable information to better reveal its origin.

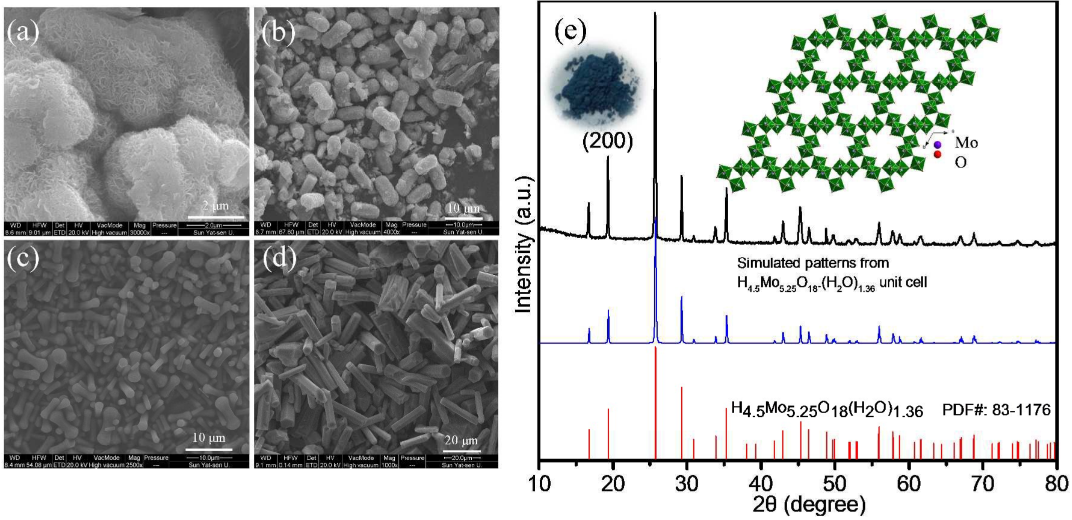

Fig. 1 The FESEM images of molybdate oxides under different reaction conditions while keeping other conditions unchanged. (a) without PVP; (b) without H_2O (c) without formic acid and HM-30 (d); (e) The corresponding XRD patterns of HM-30. The inset in (e) is a photo image of blue powders and its corresponding crystal structure of hexagonal $H_{4.5}Mo_{5.25}O_{18}\cdot(H_2O)_{1.36}$ projected along [001].

We first investigated HM-30 morphologies after 1000th cycles. Surprisingly, we found that the one-dimensional microrods were damaged completely (Fig. 4c inset). Strikingly, the result is beyond our initial expectation. Hu et al reported that the MoO_3 hydrate is a metastable phase and can be stabilized by the presence of the vanadium in view of the crystal structure perspective. Therefore, it is understandable that why the HM-30 is completely damaged. This also motivated us to explore how the phase change and morphologies evolutionary changes of the HM-30 with the charge-discharge process at different stages.

It is well-known that the *ex-situ* XRD and other advanced techniques are important tools to characterize the process of the charge-discharge. We can monitor the phase transition process of HM-30 with the charge-discharge cycles. As shown in Fig. 2a, we choose five points to illustrate the whole change process of both the phase and morphologies changes during the 1st charge-discharge process. The XRD results show that the main crystals are Li_2MoO_4 at 1.95 V, almost without remain of hexagonal $H_{4.5}Mo_{5.25}O_{18}\cdot(H_2O)_{1.36}$ crystal phase, indicating the phase change is complete (Fig. 2b). The transformation rate is also quite fast, ca. 18 min. This is the first report on how the Li_2MoO_4 nanotubes formed though the electrochemical reaction of a metastable phase $H_{4.5}Mo_{5.25}O_{18}\cdot(H_2O)_{1.36}$. Very recently, we also noticed that Zhao group reported nanotube Li_2MoO_4.[42] In the continuous lithium-ion insertion process, e.g. at 0.65, 0.34 and 0.01 V, we found that almost (211) peak position slightly shifted towards left at the 1.95, 0.65 and 3 V (Fig. 2c). Furthermore, we also found that some minor new phases produced, e.g., $LiMoO_3$, $Li_3MoO_{2.25}$, $LiMo_8O_{10}$ (denoted as $Li_xMo_yO_z$). These new minor may have an effect on the peak position of (211) peak of Li_2MoO_4. Generally, the peak position should shift towards left upon lithium-ion insertion due to the expansion of crystalline lattice.

Furthermore, we also carried out a corresponding *ex-situ* FESEM images of HM-30, as shown in the inset of Fig. 2. The results show that the HM-30 first transformed into nanotubes after lithium-ion insertion. Moreover, finally the nanotubes disappeared after discharge at 0.34 V. Very interestingly, the powder began to transform into a robust continuous film. The surface feature of the thin film looks like a slurry and gel-like materials, indicating that the pulverization particles were held together closely, which is obviously different from other previously reported literature. Actually, from the view of crystal structure, the HM-30 was changed into Li_2MoO_4 nanotube, some large volume change had occurred. It has been addressed that the crystal structure change led to the great pulverization of HM-30 in more detailed, as shown in Tab. S1.

To reveal the phase composition changes, we compared the phase composition results for HM-30 at 1st, 5th and 10th cycles. The results show that the main crystalline phase is still Li_2MoO_4, except some minor phase, such as Li_4MoO_5, $Li_4Mo_5O_{17}$, et al. (denoted as $Li_xMo_yO_z$) (Fig. 3). Surprisingly, some obvious peak shift toward low angle, indicating the continuous lithium-ion intercalation, which is different from the 1st discharge. Additionally, the peak relative intensity of Li_2MoO_4 became weak from 5th, indicating that the nanocrystalline size of Li_2MoO_4 gradually decreased. The smaller nanocrystalline size is beneficial for enhanced LIBs performance.

Based on the relative intensity of Li_2MoO_4 peak, we also noticed that the intensity of Li_2MoO_4 peak at 5th was stronger than that of Li_2MoO_4 peak after first cycle. The reason for this phenomenon may be due to high conversion reaction speed (ca. 18 min) from HM-30 to Li_2MoO_4. At this moment, freshly as-formed Li_2MoO_4 may exhibit some defects. While as the charge-discharge process continues, the crystallinity of Li_2MoO_4 began to increase till the beginning of 5th cycles, therefore, it appears a little intensive peak intensity after first cycles compared to that of after 5th cycles.

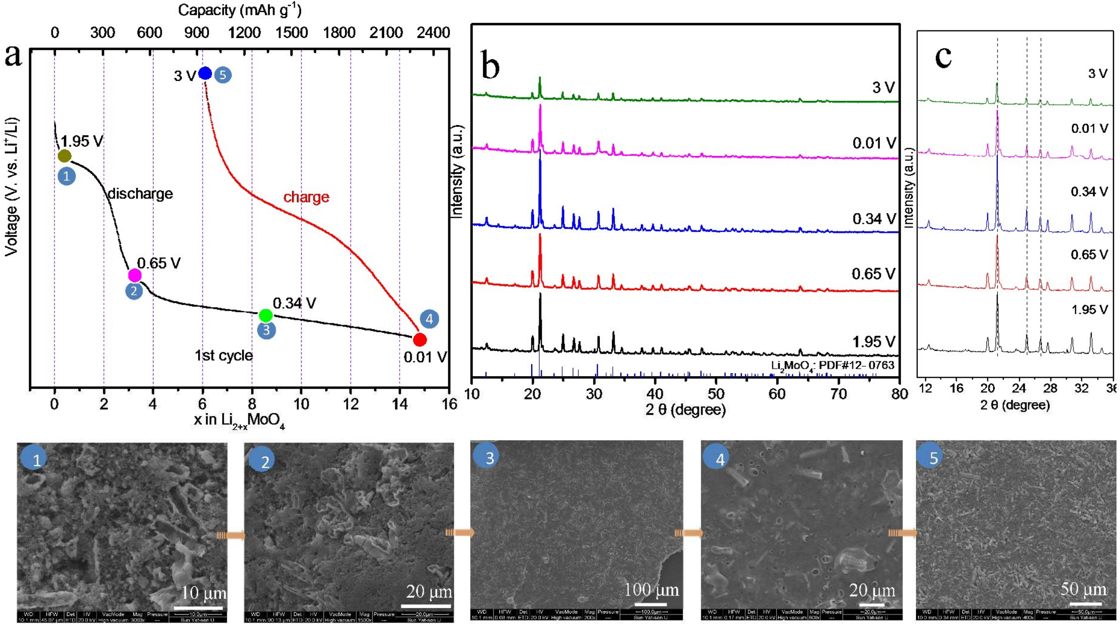

Fig. 2 The charge-discharge profile of HM-30 at the first cycle at a high current density of 2 A g^{-1} (a); (b) the corresponding XRD patterns from different stages in (a) and their peak position in the range of small angles in (b). The following *ex-situ* FESEM images are from five points in (a).

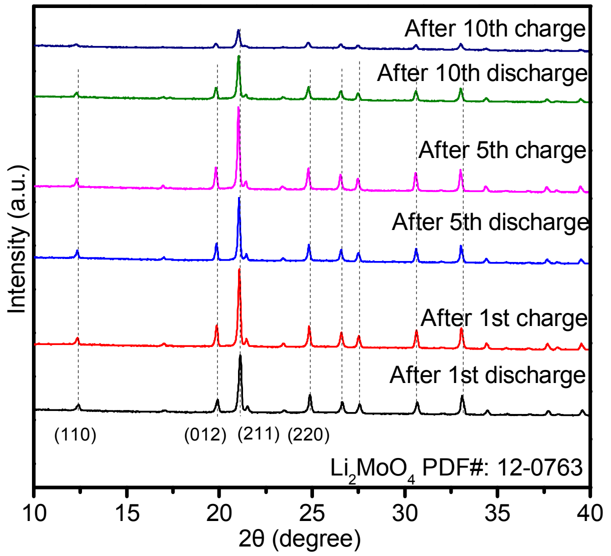

Fig. 3 XRD patterns of HM-30 after the indicated number of cycles. The current density is 2 A g^{-1}.

Moreover, for each cycle, the peak position is almost unchanged at the discharge and charge, indicating the lithium-ion insertion into Li_2MoO_4 is highly reversible, which is also further confirmed in CV curves. This is obviously different form the lithium-ion insertion (1st discharge) at 1.95 V. It is completely irreversible reaction when lithium was inserted into HM-30. In other words, the lithium-ion insertion into HM-30 is like a trigger in damaging HM-30, which gave the appropriate explanation of first fast fading of HM-30. Based on this analysis, we may conclude that the HM-30 is a metastable anode and Li_2MoO_4 is stable intermediate phase. We can reasonably infer that the high-performance LIBs may be mainly attributed to the presence of the intermediate phase Li_2MoO_4. To further reveal the superior electrochemical behaviours of HM-30 and its more detained reason in unusual extraordinary long-life cycle, we carried out other electrochemical characterizations.

The CV is a powerful tool to characterize their electrochemical behavior of HM-30. As shown in Fig. 4a, there are five obvious reduction peaks at 1.97, 1.45, 0.74, 0.38 and 1.38 V, respectively for the 1st cycle. A sharp peak at ca. 1.97 V and a broad shoulder peak at ca. 0.74 V disappeared after the first cycle, which may be due to the irreversible formation of a solid electrolyte interphase (SEI) layer, the decomposition of electrolyte and lithium-ion insertion into $[MoO_6]$ octahedron interlayer in HM. This irreversible reaction also often appeared in other MoO_3 anode systems. From the intensity of 1.97 V, it exhibits a large irreversible process, indicating the chemical reaction of HM-30 electrode materials is fast (ca. 18 min) for it to transform into Li_2MoO_4 nanotubes and SEI layer (equ. 1). It also agreed with the gel-like thin film containing Li_2MoO_4 nanotubes (Fig. 2 inset). It should be noted that the 10.5 lithium was irreversibly inserted into HM per molybdenum atoms, which is far higher than other anode materials.[2, 17, 36] Subsequently, the Li_2MoO_4 nanotubes, as intermediates, are subject to the following electrochemical reaction. (equ. 2 and 3). The reversible peaks of 1.45 and 0.38 V show that Li_2MoO_4 should be reduced and then be further oxides at 1.38 V. Based on the *ex-situ* XRD (Fig. 2 and Fig. 3) analysis, the Li_2MoO_4 is a partial reversion reaction. A partial conversion also occurred at 0.74 V (eq. 3). No obvious Mo and Li_2O was observed from the *ex-situ* XRD measurements (Fig. 2 and Fig. 3) and HRTEM (Fig. 5), however, XPS results show the presence of Mo and Li_2O (Fig. S4). The subsequent new phase $Li_{2+x}Mo_yO_4$ may generate amorphous mixture phase of metal phase Mo and Li_2O (eq. 4). Based on the above analysis; the electrochemical behaviour should include the following process:

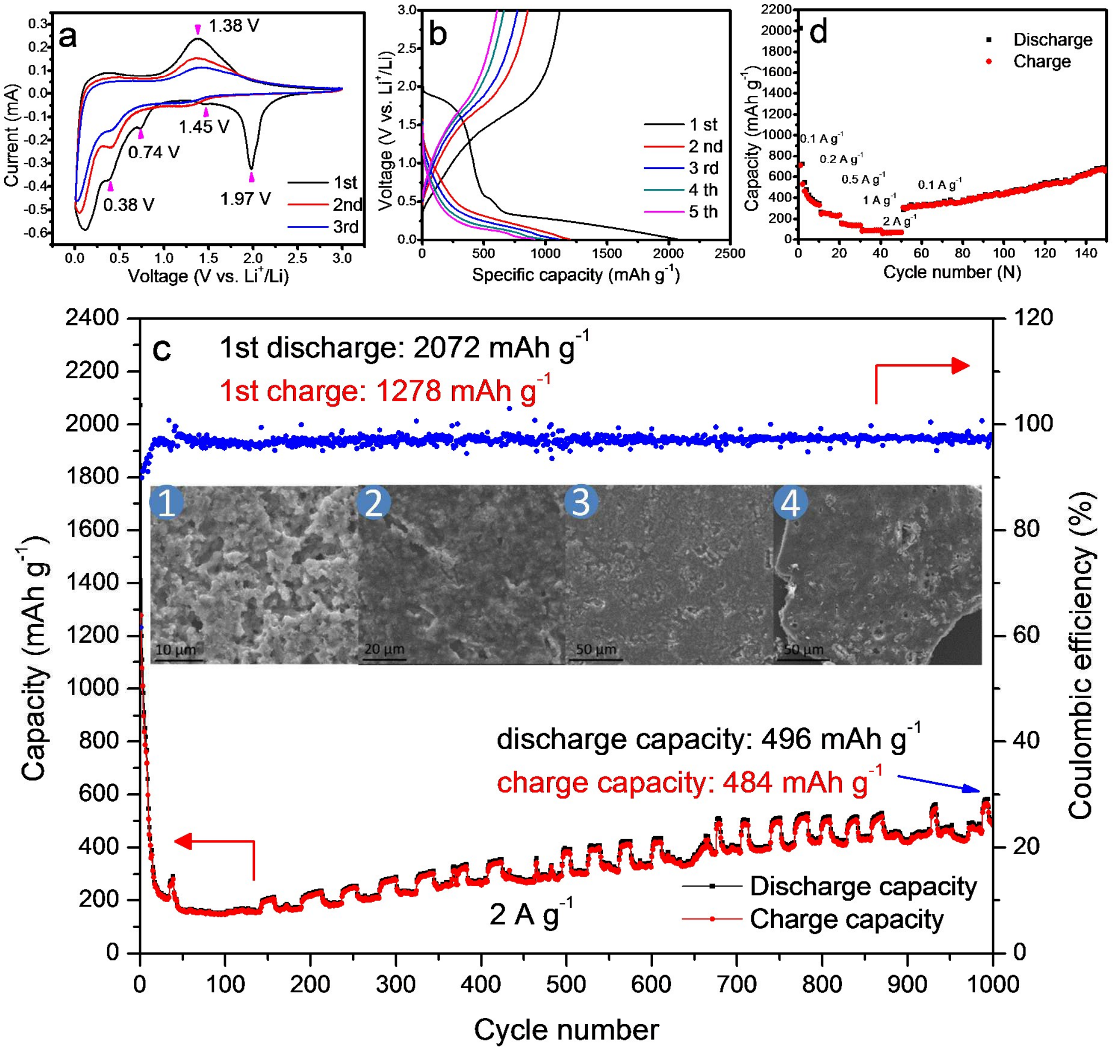

Fig. 4 (a) The CV curves of the first three cycles of HM-30; (b) the voltage profiles of HM-30 in the first five cycles at a high current density of 2 A g^{-1}. (c) the cycling performance and coulombic efficiency of HM-30 at 1000 cycles; the corresponding *ex-situ* FESEM images of HM-30 electrodes at different stages of 1000 cycles shown in the inset of (c); (d) the rate capacity of HM-30 at the different current density.

$$H_{4.5}Mo_{5.25}O_{18} \cdot (H_2O)_{1.36} + 10.5Li^+ + 10.5e^- \rightarrow 5.25Li_2MoO_4 + SEI \quad (1)$$

$$Li_2MoO_4 + xLi^+ + xe^- \leftrightarrow Li_{2+x}MoO_4 \quad (2)$$

$$Li_{2+x}MoO_4 + yLi^+ + ye^- \rightarrow Li_{2+x+y}MoO_4 \quad (3)$$

$$Li_{2+x}Mo_yO_z + 2zLi^+ + ze^- \leftrightarrow yMo + zLi_2O \quad (4)$$

Fig. 4b shows a typical charge-discharge profile of the HM-30 at a high current density of 2 A g^{-1}. The initial discharge specific capacity of HM-30 delivers an overall capacity of 2072 mAh g^{-1}, which is equivalent to an insertion of ca. 13.1 Li per formula unit according to the Faraday equation. This value is significantly higher than other oxides, e.g., 6.0 Li for Fe_2O_3, 4.4 Li for SnO_2, 2.0 Li for CoO. Although it has a high discharge specific capacity, its charge specific capacity is only 1278 mAh g^{-1} which is a little lower than that achieved in the first discharge state. From the cycle performance of HM-30 before ca. 75th cycles, as shown in Fig. 4c, we also found that the fading rate is quick. Generally speaking, the large irreversible action is due to SEI thin film, undesired electrode reaction and the decomposition of electrolyte. Surprisingly, we found that the specific capacity began to increase continuously after 75th cycles. This motivated us to explore the process of how the *ex-situ* FESEM microstructure of HM-30 with charge-discharge cycles. Based on our *ex-situ* XRD analysis in the first cycle, we found that the HM-30 can be transformed into Li_2MoO_4 very quickly. Different crystal structure and 373% large volume expansion lead to the complete pulverization of HM-30. However, it still delivered discharge capacity 496 mAh g^{-1} and charge capacity 484 mAh g^{-1} at a high current density of 2 A g^{-1}, even up to 1000th cycles. The results are quite impressive and fascinating. The results are even much higher than that of other Mo-based electrode materials.[1, 2, 5, 43-45] To the best of our knowledge, it is maximum capacity among the Mo-based electrode materials to date. It is also competitive compared with other anode materials, e.g., Fe_2O_3, SnO_2, TiO_2.[46-48]

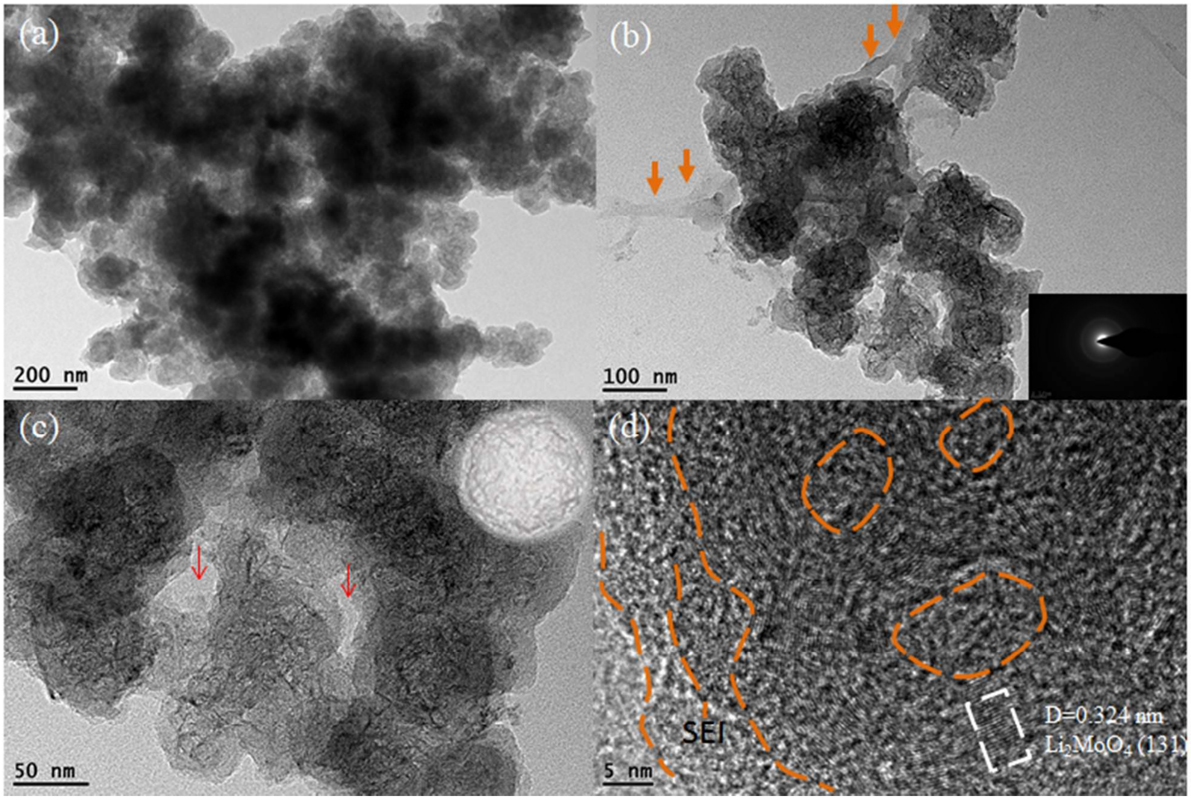

Fig. 5 The TEM images of HM-30 after charge-discharge cycling at the 1000th cycles. (a) low magnification TEM image; (b)-(c) the magnified TEM images. The inset is a schematic illustration of the nanowire of clusters encapsulated within amorphous spheres cage and (d) the HRTEM images of Li_2MoO_4 nanowire clusters showing the existence SEI thin film.

Additionally, it also exhibits an impressive rate capacity except for its superior cycling performance. Fig. 4d shows the rate behaviour of HM-30 when the current increases from 0.1 to 2 A g^{-1}. The HM-30 delivers reversible capacity of 635, 372, 241, 154, 118 mAh g^{-1} at a current density of 0.1, 0.2, 0.5, 1, 2 A g^{-1}, respectively. Surprisingly, when the current density is finally returned to its initial value of 0.1 A g^{-1}, the initial capacity is also completely recovered and increased continuously, implying the excellent tolerance for the rapid lithium-ion insertion-extraction cycles. The high capacities with long life cycles and high rate properties implied that the HM-30 is a promising anode material for LIBs application.

As shown in the inset of Fig. 4c, the *ex-situ* FESEM evolution of Li_2MoO_4 composite film was recorded. We found that the composites film looks like a gel-like thin film, which is different from the pulverization previously reported literature, which is similar to that of 1st charge-discharge (Fig. 2).

To obtain more microstructure and crystal structure information of the HM-30 powders after 1000th cycles, therefore, we took a detailed TEM analysis for the powders after 1000th cycles (Fig. 5). The results show that the whole electrode materials are composed of uniform spheres, magnified TEM of spheres reveals that some nanowires clusters were encapsulated within the spheres. The ultrathin nanowire was further verified to be Li_2MoO_4 from the HRTEM result, which agreed with the XRD results, as shown in Fig. 2 and Fig. 3. Interestingly, the mixture phase containing possible amorphous Mo and Li_2O was not observed, which is similar to the results from previous literature,[39] while a SEI thin film and other amorphous parts were observed, which acted as a cage with the role of protecting the Li_2MoO_4 nanowires. The individual sphere shows a typical amorphous structure feature, as confirmed by SAED, as shown in the inset of Fig. 5b. From the composition and structure analysis, it is similar to other materials. For another batch HM-30 sample, we also discovered the same structural feature of HM-30 after 1000th cycles (Fig. S5). A question arises from the robust gel-like thin film, how is it formed? Based on the unusually finding, we assumed that it may be the main reason for the increased capacity. This will be further discussed in Scheme 2.

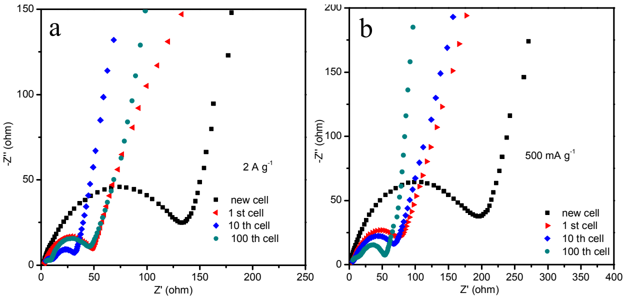

Fig. 6 The Nyquist plots of EIS of HM-30 electrodes for different cycles at the 2 A g^{-1} and 500 mA g^{-1}, respectively.

When the HM-30 electrode materials are fully pulverized, another question arises as to whether the lithium-ion diffusion paths and electronic conductive paths were maintained and how the pulverized thin film to increasingly boost LIBs performance. To answer this question, we carried out the EIS measurements with different cycles at 500 mA g^{-1} and 2 A g^{-1} to provide more information, respectively. As shown in Fig. 6, the electrode indicates a lower resistance after the 10th and 100th cycles when compared with new cell and 1st cycle cell at 2 A g^{-1} (Fig. 6a). At the low current density of 500 mA g^{-1}, the resistance decreases in a gradual way with the increase of the cycles (Fig. 6b). Surprisingly, the resistance of HM-30 electrode at 2 A g^{-1} shows a lower resistance than that at 500 mA g^{-1}. Furthermore, we also found that the wave shape cycling curves appears from ca. 150 cycles on (Fig. 4c). The results show that the robust film implied that it could maintain superior electric contact and lithium-ion transport characteristics during long charge-discharge process, indicating its unique advantages as used as anode materials, especially for high-rate LIBs. In other words, the pulverized powder did not lead to the electronic contact loss of intermediate phase Li_2MoO_4. Instead, the thin film is very helpful to the increase of capacity by lithium insertion/desertion process. For HM-30, The EIS results agree with the 1st discharge and charge capacity (Fig S1). The order of 1st capacity of HM-30 is 2 A g^{-1}> 1 A g^{-1}> 500 mA g^{-1}. The 1st capacity is higher than other Mo-based anode materials, indicating that HM are a potential electrode candidate material of LIBs.

The extraordinary long-live cycle stability may be attributed to the self-activated behaviour of the robust continuous pulverization film. Undoubtedly, the gel-like and slurry thin film played a critical role in enhancing electrochemical properties of HM-30. The *ex-situ* FESEM and TEM of the pulverized powders upon lithium-ion insertion and extraction show that it eventually was linked closely. This also gave strong evidence of the continuous conductive paths for lithium ion diffusion and electron transportation with long cycles. When the HM-30 was charged and discharged, the HM-30 was spontaneously transformed into a new phase, Li_2MoO_4 (Fig. 2b). From Fig. 2, it is obviously observed that those hollow Li_2MoO_4 nanotubes are interconnected with each other. This interconnected structure is very beneficial for LIBs stability. Surprisingly, this thin film structure is robust and stable even up to 1000 cycles. The powders often pulverized and detached from the substrate due to great volume changes, however, in our case, the film is strongly attached onto the Cu substrate (Fig.

S6). Moreover, we also found that the original HM-30 powder itself is also readily shaped (Fig. S7).

It is well-known that FTIR spectra has the ability to track the molecular structure and composition changes, to gain some extra information from the powders composition, we carried out *ex-situ* FTIR analysis for the five points presented in Fig. S8**,** The present work involves a lithium-ion battery electrolyte composition, which contains: (1) low-viscosity solvents like ethylene carbonate (EC); (2) $LiPF_6$; (3) binder, semi-crystalline polymer, Poly vinylidene fluoride (PVDF) and (4) organic solvent,1-Methyl-2-pyrrolidone (NMP). Therefore, the chemical reaction would be a very complex and unknown between the electrode materials and electrolyte. It is extremely difficult and uncertain how the reaction took place in more details. For HM-30 powders, the results show that surface of HM-30 has still three obvious OH, NH and C=C groups after hydrothermal treatment, corresponding to 3500,[49] 3200,[50] and 1610 cm^{-1},[51] respectively. It indicates that some remnants of PVP and formic acid are still adsorbed on the surface of HM-30. When discharge to 0.34 V, two new peaks with unknown organic group occur at about 3420 and 1170 cm^{-1}. The asymmetric and symmetric CH_3 bending occurs at 1430 cm^{-1}. This peak is present in all samples, indicating the powder is surrounded by organic linker-like agents. Some remnants after lithium-ion insertion and extraction also stayed on the surface of pulverized powders even when the powder was washed by DMC. It is reasonably inferred that the robust film is mainly attributed to the following factors: (1) the existence of the PVP and formic acid of HM-30 play an important role when the chemical reaction between HM-30 and electrolytes; (2) both HM-30 and Li_2MoO_4 have a wide one-dimensional tunnel for insertion and extraction of the solvated lithium-ion (Scheme. S2). The robust film like slurry was formed by "vibration" effect of insertion-extraction of lithium-ion batteries. It is hard to identify each functional group from which matter, however, the remains of organic matters still provide us some key information to address how to interconnect each other of pulverization particles.

Based on the above experimental results, a possible electrochemical mechanism is proposed to address its unique electrochemical behaviors of HM-30 (Scheme 2). First HM-30 is easily transformed into Li_2MoO_4 due to the lithium-ion intercalation (Step I). Generally speaking, the lithium-ion would easily penetrate into the one-dimensional tunnel with the solvated molecular of electrolytes due to its wide tunnel. More importantly, the surface of HM-30 contained a large amount of OH and PVP groups. During the charge-discharge process, the side reaction between the electrolyte and electrode surface easily produced SEI thin film and some unknown organic compositions. In the complex system, PVP may act as a cross link agents. Therefore, it would lead to the formation of the gel-like thin film. With the time going on, the as-formed Li_2MoO_4 nanotubes was further intercalated and gradually transformed into Li_2MoO_4 nanowire clusters by lithium-ion due to its larger ion tunnel than HM. Finally, it was evolved into ultrathin Li_2MoO_4 nanowire clusters within the Li_2O, amorphous Mo and other unknown organic film (Step II). Without doubt, the

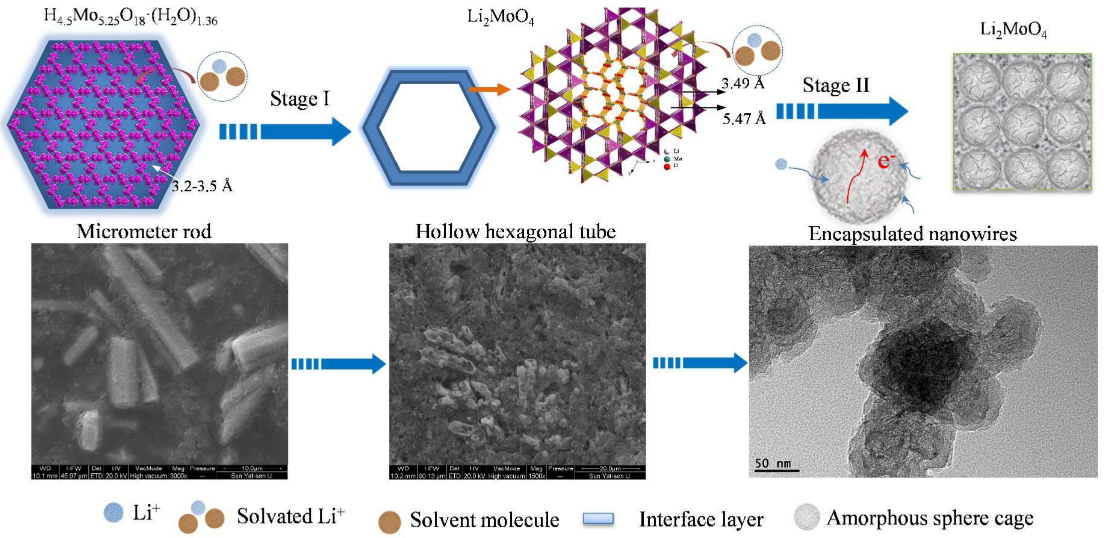

Scheme. 2 The schematic illustration of how the HM-30 was evolved into the Li_2MoO_4 nanowire clusters and amorphous spheres. The corresponding FESEM images was presented in the following of stage I and Stage II.

large exposed surface area will provide more active sites for lithium-ion diffusion and electron transfer. Moreover, the amorphous sphere acted as a carpet with 50 nm in size (Fig. 5c), yielding fast strain relaxation for effective electron and lithium-ion diffusion, thus achieving both an increased specific capacity growth with the subsequent charge-discharge process and high rate properties.

Conclusions

In summary, a novel electrode material, HM have been synthesized for the first time by a simple one-pot hydrothermal method. When tested as anode materials for LIBs, the HM indicate extraordinary long-life cycleability at a high current density of 2 A g^{-1}. Moreover, the cycle stable performance of HM retains a specific capacity of 496 mAh g^{-1} even up to 1000 cycles without any capacity fading. The extraordinary long-life cycleability at high current densities should be attributed to the following points: (1) the pulverized powder generated a high specific surface area, which is favour for the lithium-ion diffusion; (2) the robust gel-like thin film with amorphous sphere cage can effectively prohibit the aggregation of pulverization particles and reduced the strain due to the volume changes; (3) the ultrathin Li_2MoO_4 nanowire clusters formed by lithium-ion insertion/desertion provide more active sites and reduce the further pulverization upon lithium-ion insertion-extraction. In contrast to traditional method, the robust continuous gel-like pulverization film with unique combination of amorphous sphere cage and intermediate phase can effectively prohibit the mechanical and chemical pulverization of LIBs. One plausible "damage-reconstruction" model has been proposed to address the electrochemical behaviours of the HM. The results reveal that the HM are a great potential electrode material in LIBs future applications. Importantly, the proposed model may also be extended to other anode materials of LIBs and provide a new strategy for high-performance LIBs from the perspective of pulverization.

Acknowledgements

We gratefully acknowledge financial support from National Natural Science Foundation of China (No. 51462007, 41272064), and Guangxi Natural Science Foundation (No. 2014GXNSFAA118349, 2015GXNSFCA139018).

References

1 X. Yu, L. Wang, J. Liu and X. Sun, *ChemElectroChem*, 2014, **1**, 1476-1479.
2 Y. Sun, J. Wang, B. Zhao, R. Cai, R. Ran and Z. Shao, *J. Mater. Chem. A*, 2013, **1**, 4736-4746.
3 J. Zhou, N. Lin, L. Wang, K. Zhang, Y. Zhu and Y. Qian, *J. Mater. Chem. A*, 2015, **3**, 7463-7468.
4 L. Zhou, L. Yang, P. Yuan, J. Zou, Y. Wu and C. Yu, *J. Phys. Chem. C*, 2010, **114**, 21868-21872.
5 P. Meduri, E. Clark, J. H. Kim, E. Dayalan, G. U. Sumanasekera and M. K. Sunkara, *Nano Lett.*, 2012, **12**, 1784-1788.

6 W. Shi and B. A. Lu, *Electrochim. Acta*, 2014, **133**, 247-253.
7 R. Liu, D. Li, C. Wang, N. Li, Q. Li, X. Lu, J. S. Spendelow and G. Wu, *Nano Energy*, 2014, **6**, 73-81.
8 H. Song, N. Li, H. Cui and C. Wang, *Electrochim. Acta*, 2014, **120**, 46-51.
9 L. Shen, L. Yu, X. Y. Yu, X. Zhang and X. W. Lou, *Angew. Chem., Int. Ed.*, 2015, **54**, 1868-1872.
10 T. Li, X. Li, Z. Wang, H. Guo and Y. Li, *J. Mater. Chem. A*, 2015, **3**, 11970-11975.
11 Y. Chen, M. Zhuo, J. Deng, Z. Xu, Q. Li and T. Wang, *J. Mater. Chem. A*, 2014, **2**, 4449-4456.
12 J. Hwang, S. H. Woo, J. Shim, C. Jo, K. T. Lee and J. Lee, *ACS Nano*, 2013, **7**, 1036-1044.
13 H. S. Im, Y. J. Cho, Y. R. Lim, C. S. Jung, D. M. Jang, J. Park, F. Shojaei and H. S. Kang, *ACS Nano*, 2013, **7**, 11103-11111.
14 Y. H. Xu, Y. J. Zhu, Y. H. Liu and C. S. Wang, *Adv. Energy Mater.*, 2013, **3**, 128-133.
15 Y. Zhao, X. Li, B. Yan, D. Li, S. Lawes and X. Sun, *J. Power Sources*, 2015, **274**, 869-884.
16 Y. Xu, X. Zhu, X. Zhou, X. Liu, Y. Liu, Z. Dai and J. Bao, *J. Phys. Chem. C*, 2014, **118**, 28502-28508.
17 M. Liu, X. Ma, L. Gan, Z. Xu, D. Zhu and L. Chen, *J. Mater. Chem. A*, 2014, **2**, 17107-17114.
18 W. Li, J. Zheng, T. Chen, T. Wang, X. Wang and X. Li, *Chem. Commun.*, 2014, **50**, 2052-2054.
19 D. Lin, Z. Lu, P. C. Hsu, H. R. Lee, N. Liu, J. Zhao, H. Wang, C. Liu and Y. Cui, *Energy Environ. Sci.*, 2015, **8**, 2371-2376.
20 M. T. McDowell, S. W. Lee, W. D. Nix and Y. Cui, *Adv. Mater.*, 2013, **25**, 4966-4984.
21 J. Zhu, C. Gladden, N. Liu, Y. Cui and X. Zhang, *Phys. Chem. Chem. Phys.*, 2013, **15**, 440-443.
22 H. Pang, Y. Z. Zhang, W.-Y. Lai, Z. Hu and W. Huang, *Nano Energy*, 2015, **15**, 303-312.
23 H. Pang, Y. Z. Zhang, Z. Run, W.-Y. Lai and W. Huang, *Nano Energy*, 2015, **17**, 339-347.
24 Y. Z. Zhang, Y. Wang, T. Cheng, W.-Y. Lai, H. Pang and W. Huang, *Chem. Soc. Rev.*, 2015, **44**, 5181-5199.
25 Y. Song, H. Wang, Z. Li, N. Ye, L. Wang and Y. Liu, *Int. J. Hydrogen Energy*, 2015, **40**, 3613-3623.
26 J. Guo, P. Zavalij and M. S. Whittingham, *J. Solid State Chem.*, 1995, **117**, 323-332.
27 J. Kong, X. Yao, Y. Wei, C. Zhao, J. M. Ang and X. Lu, *RSC Adv.*, 2015, **5**, 13315-13323.
28 N. Wang, H. Xu, L. Chen, X. Gu, J. Yang and Y. Qian, *J. Power Sources*, 2014, **247**, 163-169.
29 M. L. Pang, J. Y. Hu and H. C. Zeng, *J. Am. Chem. Soc.*, 2010, **132**, 10771-10785.
30 R. Sharma and K. K. Kar, *Electrochim. Acta*, 2015, **156**, 199-206.
31 H. S. Toh, K. Jurkschat and R. G. Compton, *Chem.-Eur. J.*, 2015, **21**, 2998-3004.
32 J. J. Lv, J. N. Zheng, H. B. Zhang, M. Lin, A. J. Wang, J. R. Chen and J. J. Feng, *J. Power Sources*, 2014, **269**, 136-143.
33 J. J. Lv, J. N. Zheng, L. L. Chen, M. Lin, A. J. Wang, J. R. Chen and J. J. Feng, *Electrochim. Acta*, 2014, **143**, 36-43.
34 J. Yang, T. Lan, J. Liu, Y. Song and M. Wei, *Electrochim. Acta*, 2013, **105**, 489-495.
35 J. Shao, X. Li, Z. Wan, L. Zhang, Y. Ding, L. Zhang, Q. Qu and H. Zheng, *ACS Appl. Mater. Interfaces*, 2013, **5**, 7671-7675.
36 S. R. Popuri, M. Miclau, A. Artemenko, C. Labrugere, A. Villesuzanne and M. Pollet, *Inorg. Chem.*, 2013, **52**, 4780-4785.
37 Y. L. Cheah, V. Aravindan and S. Madhavi, *ACS Appl. Mater. Interfaces*, 2013, **5**, 3475-3480.
38 H. Wang, H. Yang and L. Lu, *RSC Adv.*, 2014, **4**, 43346-43350.
39 L. Li, K. H. Seng, Z. Chen, Z. Guo and H. K. Liu, *Nanoscale*, 2013, **5**, 1922-1928.
40 K. M. Shaju, F. Jiao, A. Debart and P. G. Bruce, *Phys. Chem. Chem. Phys.*, 2007, **9**, 1837-1842.
41 H. Sun, G. Xin, T. Hu, M. Yu, D. Shao, X. Sun and J. Lian, *Nat. Commun.*, 2014, **5**, 4526.
42 X. Liu, Y. Lyu, Z. Zhang, H. Li, Y. Hu, Z. Wang, Y. Zhao, Q. Kuang, Y. Dong, Z. Liang, Q. Fan and L. Chen, *Nanoscale*, 2014, **6**, 13660-13667.
43 W. X. Ji, D. Wu, R. Yang, W. P. Ding and L. M. Peng, *Chin. J. Inorg. Chem.*, 2015, **31**, 659-665.
44 L. A. Riley, S. H. Lee, L. Gedvilias and A. C. Dillon, *J. Power Sources*, 2010, **195**, 588-592.
45 D. Mariotti, H. Lindstrom, A. C. Bose and K. Ostrikov, *Nanotechnology*, 2008, **19**, 495302.
46 L. Xiao, M. Schroeder, S. Kluge, A. Balducci, U. Hagemann, C. Schulzad and H. Wiggers, *J. Mater. Chem. A*, 2015, **3**, 11566-11574.
47 X. Li, Y. Ma, L. Qin, Z. Zhang, Z. Zhang, Y. Zheng and Y. Qu, *J. Mater. Chem. A*, 2015, **3**, 2158-2165.
48 J. Shen, H. Wang, Y. Zhou, N. Ye, G. Li and L. Wang, *RSC Adv.*, 2012, **2**, 9173-9178.
49 C. Le Losq, G. D. Cody and B. O. Mysen, *Am. Mineral.*, 2015, **100**, 945-950.
50 Y. Yan, T. Kuila, N. H. Kim, S. H. Lee and J. H. Lee, *Carbon*, 2015, **85**, 60-71.
51 Y. Sun, Z. Fang, C. Wang, K. R. R. M. Ariyawansha, A. Zhou and H. Duan, *Nanoscale*, 2015, **7**, 7790-7801.

Graphical Abstract

Self-activated continuous pulverization film: an insight into the mechanism of extraordinary long-life cycleability of hexagonal $H_{4.5}Mo_{5.25}O_{18}\cdot(H_2O)_{1.36}$ microrods†

Zihua Li,[ab] Hai Wang,[*ab] Zhuangzhi Sun, [ab] Jian Su, [ab] Zuyun Wang [c] and Linjiang Wang[ab]

[a]College of Materials Science and Engineering, Guilin University of Technology, Guilin 541004, China

[b]Key Laboratory of New Processing Technology for Nonferrous Metals and Materials, Ministry of Education, Guilin University of Technology, Guilin 541004, China

[c]College of Civil Engineering and Architecture, Guilin University of Technology, Guilin 541004, China

* To whom correspondence should be addressed.

Tel: +86-773-5896-672. Fax: +86-773-5896-671. E-mail:hbwanghai@gmail.com (H Wang).

Novel hexagonal $H_{4.5}Mo_{5.25}O_{18}\cdot(H_2O)_{1.36}$ microrods (HM) exhibit an unusual and intriguing electrochemical behavior. The specific capacity of HM is first fading, then continuous increase without any capacity fading at a high current density of 2 A g^{-1}, even up to 1000 cycles, indicating its outstanding cycling performance and rate properties. A plausible mode of "damage-reconstruction" and its corresponding mechanism were provided.